Journal of Magnetism and Magnetic Materials 322 (2010) 2177–2183

Contents lists available at ScienceDirect

Journal of Magnetism and Magnetic Materials

journal homepage: www.elsevier.com/locate/jmmm

# Magnetic structure and thermodynamic properties of TmPtIn

S. Baran [a,*], D. Kaczorowski [b], A. Arulraj [c], B. Penc [a], A. Szytuła [a]

[a] M. Smoluchowski Institute of Physics, Jagiellonian University, Reymonta 4, PL-30 059 Kraków, Poland
[b] Institute of Low Temperature and Structure Research, Polish Academy of Sciences, P.O. Box 1410, PL-50 950 Wrocław, Poland
[c] Helmholtz-Zentrum Berlin, Glienicker Str. 100, D-14 109 Berlin, Germany

ARTICLE INFO

*Article history:*
Received 9 December 2009
Received in revised form
26 January 2010
Available online 6 February 2010

*Keywords:*
Rare earth intermetallics
Frustrated antiferromagnet
AF magnons
Neutron scattering

ABSTRACT

Physical properties of TmPtIn have been investigated by means of magnetic, electrical transport, calorimetric as well as neutron diffraction measurements. The compound crystallizes in the hexagonal ZrNiAl-type crystal structure. It orders antiferromagnetically below $T_N$ = 3.5 K with the Tm magnetic moments confined to the basal hexagonal plane. They form a non-collinear "triangular" magnetic structure that may be described by the propagation vector $\vec{k}=[\frac{1}{4},\frac{1}{4},\frac{1}{2}]$. At 1.6 K, the Tm magnetic moment is equal to 5.59(9)$\mu_B$. The antiferromagnetic character of the electronic ground state is reflected in the low temperature behaviors of the magnetic susceptibility and the specific heat, which may be described by spin-wave theory of antiferromagnetic magnons with linear dispersion relation. The compound exhibits metallic character of electrical conduction.



## 1. Introduction

The RPtIn (R = Sc, Y, La-Nd, Sm, Gd-Lu) intermetallic compounds crystallize in the hexagonal ZrNiAl-type structure [1–4], whereas EuPtIn crystallizes in the orthorhombic TiNiSi-type [5,6] structure. Transport and magnetic studies of RPtIn intermetallics (R = rare earth element) revealed interesting physical properties in several members of this family of compounds. CePtIn [7–10] and YbPtIn [4,11–15] were described as dense Kondo systems. No magnetic ordering was found down to 60 mK in CePtIn [7,8], while YbPtIn was reported to order antiferromagnetically below 3.4 K [11]. In PrPtIn no magnetic ordering was discovered down to 1.7 K, however the magnetic and resistivity data suggested possible ferromagnetic phase transition at lower temperatures [2]. SmPtIn was found to order ferromagnetically below 25 K [2]. Ferromagnetic ordering was also encountered in GdPtIn (below 89 K [16] or 67.5 K [13]), DyPtIn (below 38 K [16], 26.5 K [13] or 37.1 K [17]), HoPtIn (below 23.5 K [13] or 23.1 K [17]) and ErPtIn (below 8.5 K [13] or 13 K [18]). In turn, antiferromagnetic order was established in TbPtIn (below 50 K [16], 46.0 K [13,20] or 47 K [19]).

Single-crystal studies of TmPtIn were reported in Ref. [13]. The magnetic susceptibility was found to exhibit a maximum at about 4 K, typical of antiferromagnetic phase transitions, while the specific heat data yielded the transition temperature of $3.0 \pm 0.5$ K. Strong magnetic anisotropy was observed in the ordered region, with the magnetization measured in the hexagonal plane being significantly larger than that along the *c*-axis. In a field of 5.5 T, the planar component of the magnetic moment was calculated to be 4.42$\mu_B$, while the axial one was found to be equal to 2.26$\mu_B$ (at $T$ = 2 K). The angle between the easy axis and the *c*-axis was estimated to be about 72°. The inverse magnetic susceptibility yielded the value of an effective magnetic moment around 7.7$\mu_B$.

In the present work the magnetic ordering in TmPtIn has been probed by neutron powder diffraction, and the physical properties of the compound have been investigated within wide temperature range by means of magnetization, electrical resistivity and heat capacity measurements.

## 2. Experimental details

Polycrystalline sample of TmAgGe was synthesized by arc melting high-purity elements (Tm: 3N; Ag: 4N; Ge: 5N) under titanium-gettered argon atmosphere. In order to ensure appropriate homogeneity the ingot was turned over and remelted several times. Afterwards, the sample was annealed in an evacuated quartz ampoule at 600 °C for one week.

The product quality was examined by X-ray powder diffraction at room temperature on a Philips PW-3710 X'PERT diffractometer using Cu$K_\alpha$ radiation. The results confirmed the hexagonal ZrNiAl-type crystal structure and indicated almost single-phase character of the prepared sample.

Magnetic measurements were performed within the temperature range 1.7–400 K and in external magnetic fields up to 5 T using a Quantum Design SQUID magnetometer. The electrical

* Corresponding author. Tel.: +48 12 6635686; fax: +48 12 6337086.
*E-mail address:* stanislaw.baran@uj.edu.pl (S. Baran).

0304-8853/$ - see front matter © 2010 Elsevier B.V. All rights reserved.
doi:10.1016/j.jmmm.2010.02.005

resistivity was measured over the temperature interval of 3.9–290 K employing a standard dc four-probe technique and a home-made setup. Heat capacity studies were carried out in the temperature range 0.34–300 K using a relaxation method implemented in a Quantum Design PPMS platform.

The neutron powder diffraction patterns were collected within the temperature range from 1.6 to 4.1 K on the E6 diffractometer installed at the BERII reactor (Helmholtz-Zentrum Berlin). The incident neutron wavelength was 2.452 Å. The neutron diffraction data were analyzed using the Rietveld-type program FullProf [21].

## 3. Results and discussion

### 3.1. Crystal structure

The X-ray diffraction data, collected at room temperature, as well as the neutron diffraction data, obtained at 4.1 K (paramagnetic state), confirmed unambiguously the hexagonal ZrNiAl-type structure (space group $P\bar{6}2m$). In this unit cell the particular atoms occupy the following sites:

| | | | |
|---|---|---|---|
| 3 Tm atoms at 3(g) site | $x_{Tm}, 0, \frac{1}{2}$ | $0, x_{Tm}, \frac{1}{2}$ | $\bar{x}_{Tm}, \bar{x}_{Tm}, \frac{1}{2}$ |
| 3 In atoms at 3(f) site | $x_{In}, 0, 0$ | $0, x_{In}, 0$ | $\bar{x}_{In}, \bar{x}_{In}, 0$ |
| 2 Pt atoms at 2(c) site | $\frac{1}{3}, \frac{2}{3}, 0$ | $\frac{2}{3}, \frac{1}{3}, 0$ | |
| 1 Pt atom at 1(b) site | $0, 0, \frac{1}{2}$ | | |

**Table 1**
Refined structural parameters of TmPtIn together with residuals for profile and integrated intensities.

| | |
|---|---|
| $a$ (Å) | 7.594(3) |
| $c$ (Å) | 3.769(2) |
| $c/a$ | 0.4963(3) |
| $V$ (Å$^3$) | 188.2(2) |
| $x_{Tm}$ | 0.590(2) |
| $x_{In}$ | 0.281(5) |
| $\chi^2$ | 1.90 |
| $R_{profile}$ (%) | 2.20 |
| $R_{Bragg}$ (%) | 5.31 |

The parameters were derived from neutron diffraction patterns collected at 4.1 K.

The values of the lattice parameters and the free positional parameters $x$, derived from the neutron diffraction pattern, are listed in Table 1.

### 3.2. Magnetic behavior

The magnetic properties of TmPtIn are presented in Fig. 1. Above about 60 K, the inverse magnetic susceptibility exhibits a linear-in-T behavior. At lower temperatures some curvature in $\chi^{-1}(T)$ is seen, presumably due to CEF effect. Fitting the Curie–Weiss formula to the experimental data yielded the paramagnetic Curie temperature $\theta_p = 6.5(2)$ K and the effective magnetic moment $\mu_{eff} = 7.65(3)\mu_B$. Nearly identical $\mu_{eff}$ was reported for both characteristic crystallographic directions in single-crystalline TmPtIn [13]. This value is close to that expected for a free $Tm^{3+}$ ion ($7.56\mu_B$). As shown in the upper inset in Fig. 1, the magnetic susceptibility has a maximum typical for antiferromagnetic phase transition. The critical temperature equal to 3.4 K was identified from the maximum in the derivative $d(\chi_m T)/dT$. The antiferromagnetic character of the magnetic ordering is corroborated by the behavior of the isothermal magnetization taken at 1.72 K as a function of magnetic field up to about 5 T. A clear metamagnetic transition is visible at $B$ = 0.5 T (see the lower inset to Fig. 1). The saturation magnetic moment in the field-induced ferromagnetic state at 1.72 K equals $4.5(2)\mu_B$, i.e. it is much smaller than the free $Tm^{3+}$ ion value ($7.0\mu_B$) and should be related to the CEF ground state of the compound. Very similar magnetization characteristics were reported in Ref. [13] for TmPtIn single crystal measured in magnetic field applied within the *ab* plane of its hexagonal unit cell.

### 3.3. Electrical resistivity

The results of electrical transport measurements of TmPtIn are presented in Fig. 2. The compound exhibits metallic behavior with the room temperature resistivity of about 210 μΩ cm that decreases down to about 130 μΩ cm at 3.9 K, the terminal temperature in this study. Remarkably, as is apparent from Fig. 2, very similar overall temperature dependence of the resistivity is observed for the nonmagnetic analog LaPtIn, which

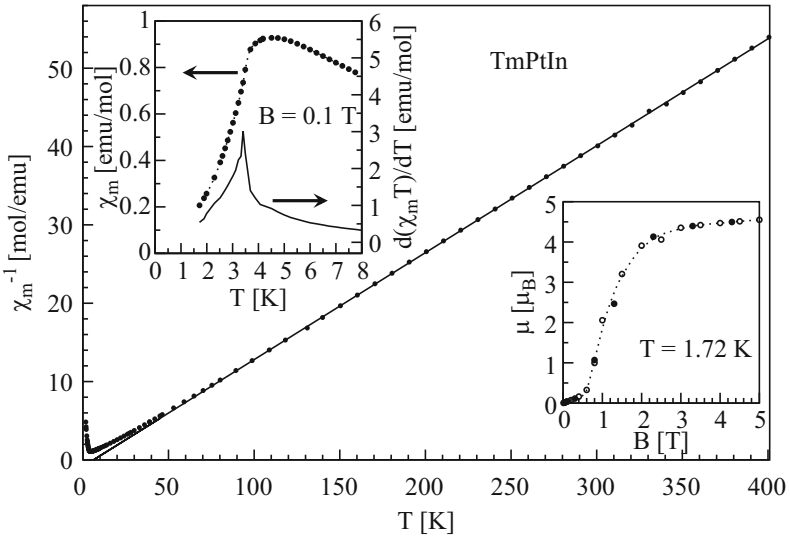


**Fig. 1.** Inverse magnetic susceptibility of TmPtIn. The solid line shows the Curie–Weiss fit discussed in text. The upper-left corner inset presents magnetic susceptibility at low temperatures together with the derivative $d(\chi_m T)/dT$. The bottom-right corner inset presents isothermal magnetic moment per formula unit during increasing (open symbols) and decreasing (filled symbols) of the magnetic field.

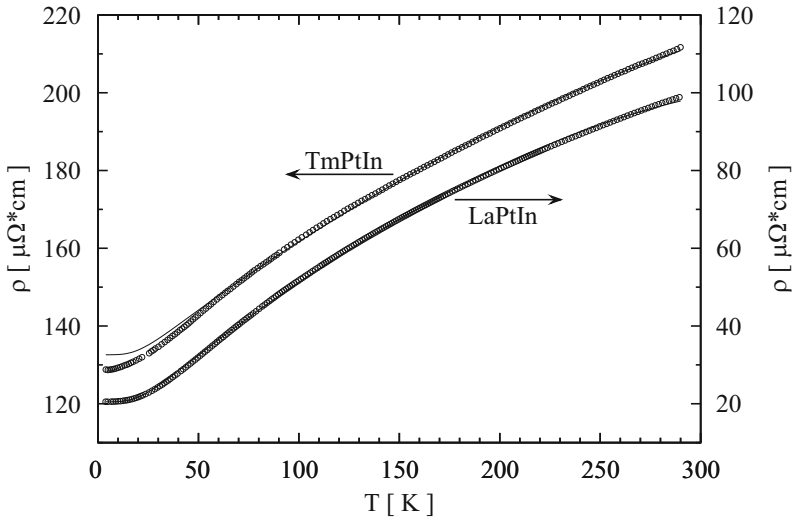


**Fig. 2.** Electrical resistivity of LaPtIn (right axis) and TmPtIn (left axis). The solid lines represent the fits to the Bloch–Grüneisen–Mott formula (see the text for details).

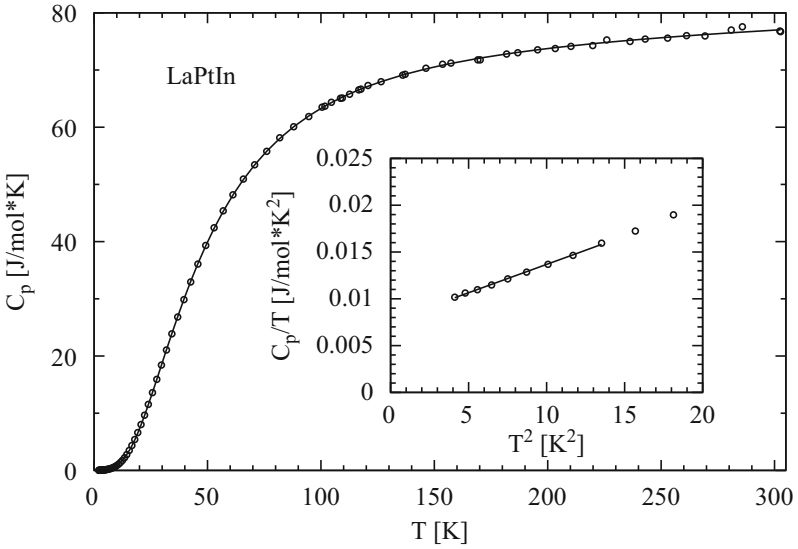


**Fig. 3.** Specific heat of LaPtIn (open symbols). The solid line shows the fit to the formula given by Eq. (3) (see main text for details). The inset presents the low-temperature part of $C_p/T$ dependence on $T^2$. The solid line shows the linear fit used to derive the value of an electronic specific heat coefficient $\gamma$.

indicates that $\rho(T)$ of TmPtIn is mainly governed by temperature related changes in the phonon scattering of the conduction electrons. The resistivity of a nonmagnetic metallic compound may be described by the so-called Bloch–Grüneisen–Mott (BGM) formula:

$$\rho(T) = \rho_0 + 4RT\left(\frac{T}{\Theta_D}\right)^4 \int_0^{\Theta_D/T} \frac{x^5\,\mathrm{d}x}{(e^x-1)(1-e^{-x})} - KT^3 \qquad (1)$$

where $\rho_0$ is the residual resistivity due to scattering the conduction electrons on static defects of the crystal lattice, the second term accounts for electron–phonon scattering processes and the third term represents the s-d interband scattering. Fitting Eq. (1 to the experimental data of LaPtIn gives the following set of parameters: $\rho_0 = 20.5(4)\,\mu\Omega\,\mathrm{cm}$, $R = 0.3469(2)\,\mu\Omega\,\mathrm{cm/K}$, $\Theta_D = 131.3(5)\,\mathrm{K}$ and $K = 9.14(1)\cdot 10^{-7}\,\mu\Omega\,\mathrm{cm/K^{-3}}$. The parameter $\Theta_D$ is usually treated as a rough estimation of the Debye temperature, despite its value is influenced in some way by electronic correlations [23]. In the case of LaPtIn the so-obtained $\Theta_D$ appears to be in good agreement with the value estimated from the specific heat data (see section *Specific heat* for details).

To account for possible little differences in the non-magnetic contributions to the electrical resistivity of LaPtIn and TmPtIn (especially as regards the Mott's interband scattering), the $\rho(T)$ data of the latter compound were independently analyzed in terms of Eq. (1) with an added term $\rho_\infty$ that represents scattering the conduction electrons on disordered magnetic moments. The evaluation was made above 50 K, i.e. in the temperature range where $\rho_\infty$ can be assumed to be temperature independent (at high temperatures $\rho(T)$ is dominated by the phonon contribution and CEF effects are nearly negligible). In order to reduce the number of fit parameters, the Debye temperature in TmPtIn was fixed at a value of 127.2(5) K derived from $\Theta_D$ found for LaPtIn using a general formula:

$$\Theta_{R'_mM_nX_p} = \Theta_{R_mM_nX_p}\left(\frac{m(M_R)^{3/2} + n(M_M)^{3/2} + p(M_X)^{3/2}}{m(M_{R'})^{3/2} + n(M_M)^{3/2} + p(M_X)^{3/2}}\right)^{1/3} \qquad (2)$$

where $M'_R$, $M_R$, $M_M$ and $M_X$ are the molecular masses of the respective elements, while $m$, $n$ and $p$ are natural numbers representing the stoichiometry. The least-squares fit is shown in Fig. 2, and the so-obtained parameters are: $\rho_0+\rho_\infty = 132.60(5)\,\mu\Omega\,\mathrm{cm}$, $R = 0.3239(5)\,\mu\Omega\,\mathrm{cm/K}$ and $K = 6.10(5)\cdot 10^{-7}\,\mu\Omega\,\mathrm{cm/K^{-3}}$. Apparently, the values of $R$ and $K$ are very close to those determined for LaPtIn, and thus corroborate the similarity in the electron–phonon and interband electron-electron scattering processes. In turn, the distinct difference between $\rho_0$ found for LaPtIn and the sum $\rho_0+\rho_\infty$ derived for TmPtIn is due to the magnetic contribution present in the latter compound but it may also reflect enhanced residual scattering because of insufficient metallurgical quality of the TmPtIn specimen studied. Indeed, the measured sample was very brittle and contained some microcracks, which probably influenced $\rho_0$. It is also possible that the observed difference is partially caused by polycrystalline character of the two samples, in which some preferred orientation of grains may be expected owing to anisotropic character of their crystal structure.

Below 50 K, the experimental resistivity of TmPtIn is smaller than the calculated one due to reduction in the scattering on the CEF levels which accompanies their gradual depopulation with decreasing temperature. Here, it is worth to recall that also the magnetic susceptibility of TmPtIn indicates the CEF effect in a similar temperature region.

### 3.4. Specific heat

Fig. 3 presents the temperature dependence of the specific heat of LaPtIn. At low temperatures the ratio $C_p/T$ varies as $(T^2)$, which provides from the formula $C_p/T = \gamma+\beta T^2$ an electronic specific heat coefficient $\gamma$ equal to 7.62 mJ/mol*K$^2$ (see the inset in Fig. 3). This value of $\gamma$ is typical for nonmagnetic metallic compounds. For

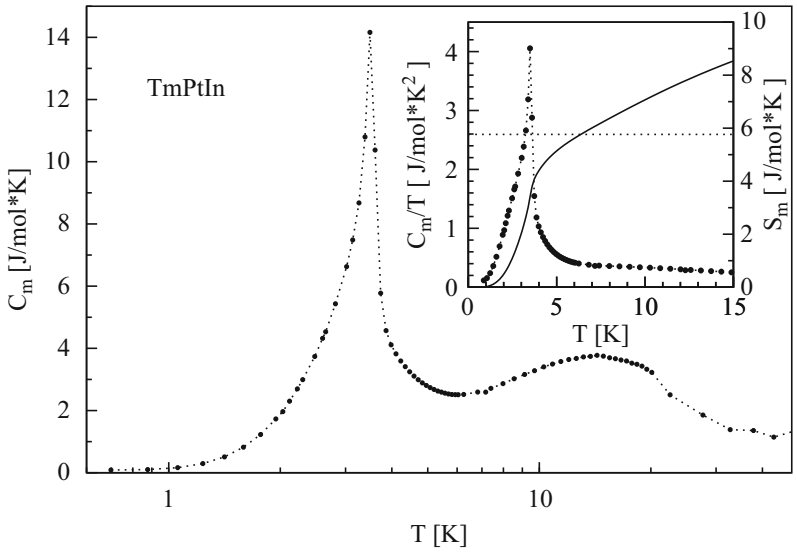


**Fig. 4.** Temperature dependence of a magnetic contribution to the specific heat of TmPtIn. The inset presents the low-temperature part of $C_m/T$ (dots) and magnetic entropy $S_m$ (solid line). The entropy level $R\ln 2$ is marked by dotted line.

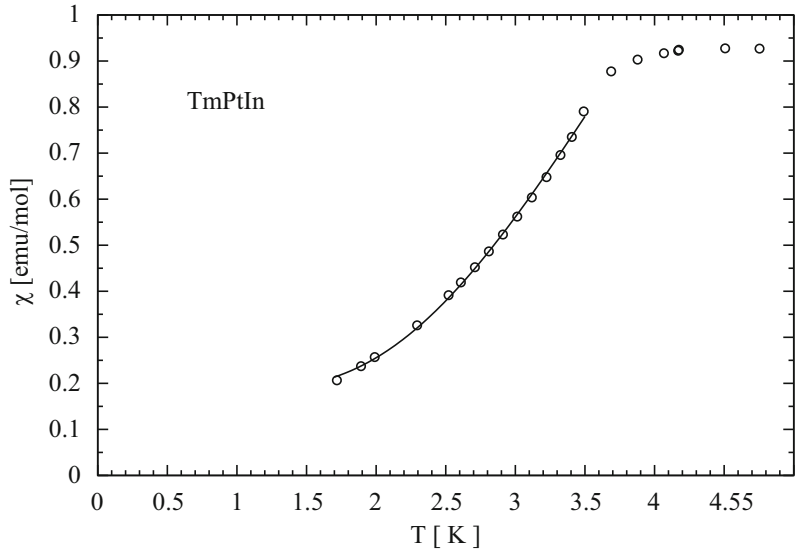


**Fig. 5.** The fit of the formula given by Eq. (4) to the experimental data of TmAgGe magnetic susceptibility.

example, for the isostructural phase YPtIn $\gamma$ was reported to be 6.7 mJ/mol*K$^2$ [22]. In a wide temperature range the specific heat of LaPtIn can be described by the formula that accounts for the electronic and phonon contributions:

$$C_{ph+el} = 9R\frac{1}{1-\alpha T}\left(\frac{T}{\Theta_D}\right)^3 \int_0^{\frac{\Theta_D}{T}} \frac{x^4 e^x}{(e^x-1)^2}\,dx + R\frac{1}{1-\alpha T}\sum_i \frac{\left(\frac{\Theta_{E_i}}{T}\right)^2 e^{\Theta_{E_i}/T}}{\left(e^{\Theta_{E_i}/T}-1\right)^2} + \gamma T \tag{3}$$

where $\Theta_D$ is the Debye temperature, $\Theta_{E_i}$ are the Einstein temperatures, $\alpha$ is the anharmonic coefficient and $R$ is the gas constant. Assuming that the Einstein temperatures can be grouped into 2 branches, each of multiplicity 3, one obtains a satisfactory fit of the experimental data of LaPtIn with the parameters: $\Theta_D = 131(2)$ K, $\Theta_{E_1} = 131(2)$ K, $\Theta_{E_2} = 210(2)$ K and $\alpha = 6.43(23)\cdot 10^{-5}$ 1/K ($\gamma$ was fixed at the value found from the low-temperature analysis).

In order to analyze the specific heat of TmPtIn, first the characteristic temperatures of the phonon contributions were calculated using Eq. (2) with the input Debye and Einstein parameters as found for LaPtIn. This way the following values were derived: $\Theta_D = 127(2)$ K, $\Theta_{E_1} = 127(2)$ K and $\Theta_{E_2} = 203(2)$ K. Then, assuming that also the electronic contribution to the specific heat of TmPtIn is similar to that determined for its nonmagnetic counterpart, the temperature variation of $C_{ph+el}$ in TmPtIn was derived from Eq. (3). Finally, subtracting the so-estimated sum of the phonon and electronic contributions from the experimental $C_p$ data the magnetic specific heat $C_m(T)$ was obtained, as shown in Fig. 4).

At the temperature of about 3.5 K, a sharp lambda-shaped anomaly is seen, which is related to the antiferromagnetic ordering. The jump in the specific heat $\Delta C_p$ at $T_N$ equals approximately 12 J/mol*K, which is smaller that the theoretical value of 20.54 J/mol*K, given by the mean field theory relation $\Delta C_m(T_N) = 2.5R((2J+1)^2-1)/((2J+1)^2+1)$ (Ref. [24]) with $J$ = 6 corresponding to the entire multiplet of the $Tm^{3+}$ ion. However, the experimental value of $\Delta C_m(T_N)$ is very close to the value of 12.47 J/mol*K, appropriate for a doubly degenerated ($J$ = 1/2) CEF ground state.

The temperature variation of the magnetic entropy $S_m(T)$, derived from the $C_p/T$ dependence (see the inset to Fig. 4), exhibits a distinct change in slope at the Neel temperature with the entropy reaching a value of $R\ln 2$, which also hints at the ground state being a doublet or two closely separated singlets. In the unit cell of TmPtIn, the $Tm^{3+}$ ions are located at the crystallographic position 3$g$ with the orthorhombic point symmetry $C_{2v}$ (mm2). In the crystal field potential of this symmetry the thulium $^3H_6$ ground multiplet splits into several energy levels, with 13 singlets being the terminal case with total lifting of the $2J+1 = 13$ degeneracy. Such a distribution of the crystal field levels was found for the isostructural compound TmNiAl [25]. Inelastic neutron diffraction experiment is necessary to conclude on the crystal field splitting scheme in TmPtIn.

### 3.5. Low temperature thermodynamic properties—AF magnons evidence

The spin-wave theory of antiferromagnetic magnons with linear dispersion relation $\varepsilon^2(k) = \Delta^2 + Dk^2$, where $\Delta$ denotes an energy gap in the magnons spectrum and $D$ is the spin-wave stiffness, predicts the following temperature dependence of the average magnetic susceptibility in the ordered state [26]

$$\chi(T) = \tfrac{1}{3}(\chi_{\parallel} + 2\chi_{\perp}) = A + B\sqrt{\Delta T}e^{-\Delta/T}(\Delta - T) \tag{4}$$

In this equation $\chi_{\parallel}$ and $\chi_{\perp}$ stand for the axial and planar components of the magnetic susceptibility, respectively, while $A$ and $B$ are constants. It is worth to note that the parameter $A$ is proportional to $1/\beta$, where $\beta$ is an anisotropy constant.

Fitting Eq. (4) to the experimental data of TmPtIn below 3.5 K (see Fig. 5) yielded the following parameters: $A$=0.184(7) [emu/mol], $B$=0.262(4) [emu/mol*K$^2$] and $\Delta = 9.62(24)$ K.

In turn, the formula predicted by the spin-wave theory for the temperature variation of the magnetic specific heat in the ordered region is given by expression [26]:

$$C_m(T) = cT^{-1/2}e^{-\Delta/T} \tag{5}$$

where $c$ is a constant.

Fitting Eq. (5) to the low-temperature specific heat data of TmPtIn gave the parameters: $c = 167(10)\,\mathrm{J} * \mathrm{K}^{1/2}/\mathrm{mol}$ and $\Delta = 8.25(14)$ K. As seen in Fig. 6, the fit represents well the data below 2.8 K but at higher temperatures no satisfactory description was obtained. It is worth to note that the obtained values of $\Delta$ are close to one another, thus supporting the appropriateness of the analyzes made. Similar description of the magnetic susceptibility and the specific was previously proposed for the isostructural

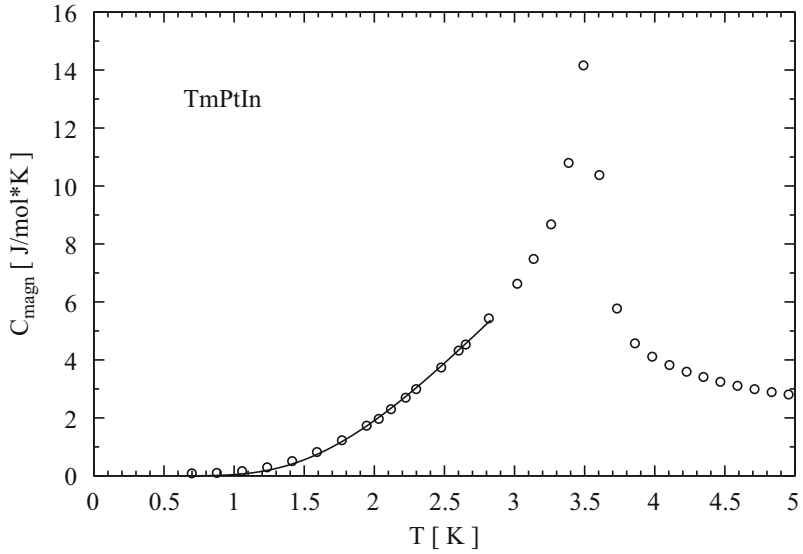


**Fig. 6.** The fit of the formula given by Eq. (5) to the experimental data of TmPtIn specific heat.

compounds TbAuIn [27] and TmAgGe [28]. In the two latter antiferromagnets the spin-wave gaps are of similar magnitude as that found for TmPtIn.

### 3.6. Magnetic structure

The neutron diffraction patterns of TmPtIn taken below the Néel temperature clearly reveal the presence of some additional reflections due to the magnetic ordering. The magnetic contribution can be easily extracted by making differential pattern, like the one shown in Fig. 7. All the Bragg reflections of magnetic origin can be indexed using the propagation vector $\vec{k}=[\frac{1}{4},\frac{1}{4},\frac{1}{2}]$.

In order to reduce theoretically infinite number of possible magnetic moment arrangements, a group theory analysis was performed. The magnetic structures allowed by symmetry were calculated with the use of the computer program *MODY* [29]. Magnetic moments of each magnetic structure allowed by symmetry have to be parallel to basic vectors (BV) of irreducible representations (IR). For a particular propagation vector the magnetic moments are divided into so-called orbits. Within one orbit the magnetic moments have to be of same magnitude, while the magnitude of magnetic moments in a different orbit may be different (they are mutually independent from the symmetry point of view).

Table 2 lists all the allowed basic vectors, in case of the space group $G=P\bar{6}2m$, the propagation vector $\vec{k}=[\frac{1}{4},\frac{1}{4},\frac{1}{2}]$ and three rare earth magnetic moments present in the crystallographic unit cell, i.e. $Tm_1$ at $x_{Tm},0,\frac{1}{2}$, $Tm_2$ at $1-x_{Tm},1-x_{Tm},\frac{1}{2}$ and $Tm_3$ at $0,x_{Tm},\frac{1}{2}$, where $x_{Tm}=0.590(2)$ (see also Table 1). The magnetic moments of $Tm_1$ and $Tm_3$ belong to the 1st orbit, while the moment of $Tm_2$ belongs to the 2nd orbit. When examining Table 2, it should be noted that irreducible representation $\tau_1$ appears twice for the 1st orbit (it is denoted as $\tau_1$ and $\tau_1'$), whereas it appears only once for the 2nd orbit. Similar behavior was found for $\tau_3$. In turn, the irreducible representation $\tau_2$ appears only for the 1st orbit, while for the 2nd one it is missing.

The best fit to the experimental diffraction data was found for an arrangement of the magnetic moments that refers to the basic vectors of $\tau_1$. The calculated pattern is shown in Fig. 7 together with the experimental data, while the magnetic structure itself is presented in Fig. 8. All the magnetic moments are confined in the basal hexagonal plane. The adjacent (0 0 1) planes are coupled antiferrromagnetically. The magnetic structure is a typical "triangular" one, often found in magnetically frustrated systems. At 1.6 K, the Tm magnetic moment equals $5.59(9)\mu_B$. The temperature variation of this moment is shown in the inset to Fig. 7. The refined magnetic structure parameters are summarized in Table 3.

## 4. Discussion

The results presented in this work proved the existence of antiferromagnetic ordering in TmPtIn at low temperatures. The specific heat and neutron diffraction data provided the Néel temperature equal to 3.5 K while the magnetic susceptibility equal to 3.4 K. The transition temperature is close to the value 3.0(5) K reported from single-crystal studies [13]. The strong magnetic anisotropy suggesting the planar component of magnetization to dominate [13] was confirmed by our neutron diffraction data. The magnetic structure model that fits best the experimental data consists of only planar component of magnetic moment.

Authors of Ref. [13] suggest that within the basal plane magnetic moments should be confined along [2 1 0] direction and its equivalents (i.e. [2 1 0], [$\bar{1}$ 1 0], etc.). However, testing the magnetic structure models, allowed by symmetry, performed in this work did not confirm this hypothesis. The best structure model has magnetic moments parallel to [1 0 0], [1 1 0] and [0 1 0] directions.

The magnetic moment of $5.59(9)\mu_B$ at 1.6 K found from neutron diffraction is smaller then the free $Tm^{3+}$ ion which

**Table 2**
Basic vectors (BV) of the irreducible representations (IR).

| PV | $\vec{k}'=[\frac{1}{4},\frac{1}{4},\frac{1}{2}]$ | | |
|---|---|---|---|
| IR | 1st orbit | | 2nd orbit |
| | $Tm_1$ | $Tm_3$ | $Tm_2$ |
| $\tau_1$ | [1,0,0] | [0,1,0] | [1,1,0] |
| $\tau_1'$ | [0,1,0] | [1,0,0] | |
| $\tau_2$ | [0,0,1] | [0,0,−1] | – |
| $\tau_3$ | [1,0,0] | [0,−1,0] | [1,−1,0] |
| $\tau_3'$ | [0,1,0] | [−1,0,0] | |
| $\tau_4$ | [0,0,1] | [0,0,1] | [0,0,1] |

Abbreviation PV denotes propagation vector.

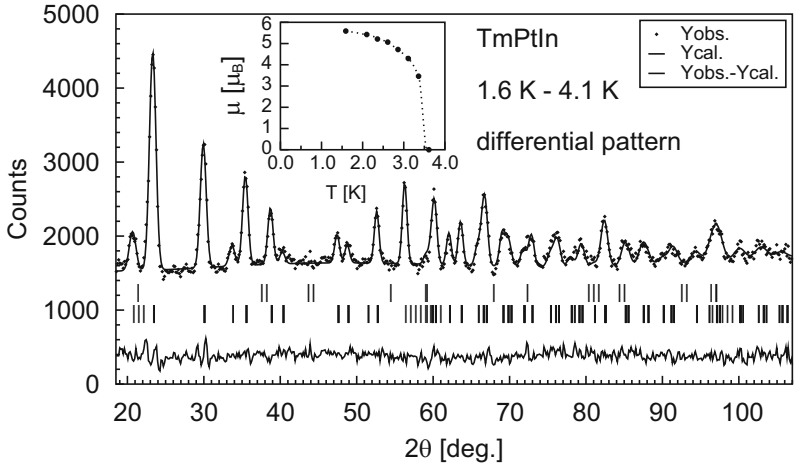


**Fig. 7.** Differential neutron diffraction pattern of TmPtIn together with Rietveld fit and difference plot. The pattern was made as a difference between patterns collected at 1.6 and 4.1 K. The upper row of vertical ticks indicates the positions of nuclear reflections (it is ploted just as a reference because nuclear reflections are absent in differential pattern). The next row indicates the positions of reflections originating from antiferromagnetic order. The inset presents the temperature dependence of amplitude of modulation of magnetic moment.

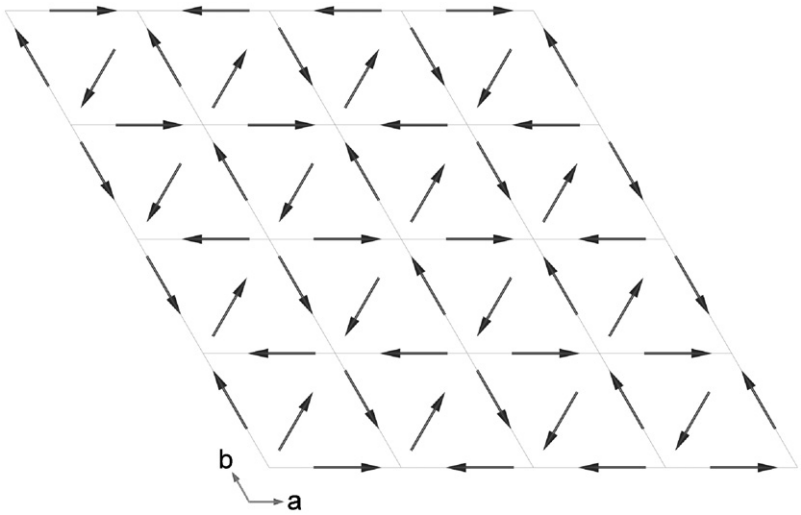


**Fig. 8.** The antiferromagnetic structure of TmPtIn derived from neutron diffraction. The adjacent (0 0 1) planes are coupled antiferrromagnetically.

**Table 3**
Refined parameters of TmPtIn magnetic structure together with residuals for profile and integrated magnetic intensities.

| Atom | $Tm_1$ | $Tm_2$ | $Tm_3$ |
|---|---|---|---|
| PV | $\vec{k}=[\frac{1}{4},\frac{1}{4},\frac{1}{2}]$ | | |
| orbit | 1 | 2 | 1 |
| DMM | [1 0 0] | [1 1 0] | [0 1 0] |
| $\mu$ ($\mu_B$) | 5.59(9) | | |
| $\chi^2$ | 2.10 | | |
| $R_{profile}$ (%) | 2.57 | | |
| $R_{magnetic}$ (%) | 8.53 | | |

The parameters were derived from the differential neutron diffraction pattern made as difference between patterns collected at 1.6 and 4.1 K. PV denotes propagation vector while DMM direction of magnetic moment.

equals $7.0\mu_B$, however, it is still larger than the values found from magnetization measurements: $4.5(2)\mu_B$ at $B=5$ T and $T=1.72$ K for polycrystalline sample (see *Magnetic behavior* section) and $4.42\mu_B$ at $B=5.5$ T and $T=2$ K (single-crystal with magnetic field applied along [1 2 0] direction [13]). The difference between magnetic moment derived from neutron diffraction and magnetization measurements suggests that the full saturation has not been reached under external magnetic field of 5 T and temperature close to 2 K.

## Acknowledgments

This research project has been supported by the European Commission under the 6th Framework Programme through the Key Action: Strengthening the European Research Area, Research Infrastructures. Contract no: RII3-CT-2003-505925 (NMI3) and by the National Scientific Network "Strongly correlated materials: preparation, fundamental research and applications".

## References

[1] R. Ferro, R. Marazza, G. Rambaldi, Z. Anorg. Allg. Chem. 410 (1974) 219–224.
[2] V.I. Zaremba, Y.V. Galadzhun, B.D. Belan, A. Pikul, J. Stêpień-Damm, D. Kaczorowski, J. Alloys Comp. 316 (2001) 64–69.
[3] Y.V. Galadzhun, V.I. Zaremba, H. Piotrowski, P. Mayer, R.-D. Hoffmann, R. Pöttgen, Z. Naturforsch. 55 b (2000) 1025–1030.
[4] D. Kaczorowski, B. Andraka, R. Pietri, T. Cichorek, V.I. Zaremba, Phys. Rev. B 61 (2000) 15255–15261.
[5] R. Pöttgen, Z. Krist. 211 (1996) 884–890.
[6] R. Müllmann, B.D. Mosel, H. Eckert, G. Kotzyba, R. Pöttgen, J. Solid State Chem. 137 (1998) 174–180.
[7] T. Fujita, K. Satoh, Y. Maeno, Y. Uwatoko, H. Fujii, J. Magn. Magn. Mater. 76-77 (1988) 133–134.
[8] K. Satoh, T. Fujita, Y. Maeno, Y. Uwatoko, H. Fujii, J. Phys. Soc. Jpn. 59 (1990) 692–700.
[9] Y. Yamaguchi, J. Sakurai, F. Teshima, H. Kawanaka, T. Takabatake, H. Fujii, J. Phys.: Condens. Matter 2 (1990) 5715–5721.
[10] M. Kurisu, T. Takabatake, H. Fujii, J. Magn. Magn. Mater. 90–91 (1990) 469–470.
[11] O. Trovarelli, C. Geibel, R. Cardoso, S. Mederle, R. Borth, B. Buschinger, F.M. Grosche, Y. Grin, G. Sparn, F. Steglich, Phys. Rev. B 61 (2000) 9467–9474.
[12] S. Yoshii, K. Kindo, K. Katoh, Y. Niide, A. Ochiai, J. Magn. Magn. Mater. 272–276 (2004) e99–e100.
[13] E. Morosan, S.L. Bud'ko, P.C. Canfield, Phys. Rev. B 72 (2005) 014425.
[14] E. Morosan, S.L. Bud'ko, Y.A. Mozharivskyj, P.C. Canfield, Phys. Rev. B 73 (2006) 174432.
[15] P. Bonville, M. Rams, K. Królas, J.-P. Sanchez, P.C. Canfield, O. Trovarelli, C. Geibel, Eur. Phys. J. B 55 (2007) 77–84.
[16] K.C. Watson, J. Crangle, K.-U. Neumann, K.R.A. Ziebeck, J. Magn. Magn. Mater. 140–144 (1995) 883–884.
[17] S. Baran, Ł. Gondek, J. Hernández-Velasco, D. Kaczorowski, A. Szytuła, J. Magn. Magn. Mater. 305 (2006) 196–201.
[18] S. Baran, Ł. Gondek, J. Hernández-Velasco, D. Kaczorowski, A. Szytuła, J. Magn. Magn. Mater. 300 (2006) 484–489.
[19] O. Garlea, E. Morosan, S.L. Bud'ko, J.L. Zarestky, P.C. Canfield, C. Stassis, J. Appl. Phys. 95 (2004) 6921–6923.
[20] E. Morosan, S.L. Bud'ko, P.C. Canfield, Phys. Rev. B 71 (2005) 014445.
[21] J. Rodriguez-Carvajal, Physica B 192 (1993) 55–69.
[22] G.D. Samolyuk, S.L. Bud'ko, E. Morosan, V.P. Antropov, P.C. Canfield, J. Phys.: Condens. Matter 18 (2006) 1473–1482.
[23] M. Giovannini, H. Michor, E. Bauer, G. Hilscher, P. Rogl, R. Ferro, J. Alloys Compds. 280 (1998) 26–38.
[24] J.G. Sereni, Magnetic systems: specific heat, in: K.H. Buschow, E. Gratz (Eds.), Encyclopedia of Materials, Science Technology, vol. 5, Elsevier Science, New York, 2001, pp. 4986–4994.
[25] N.C. Tuan, V. Sechovský, M. Diviš, P. Svoboda, H. Nakotte, F.R. de Boer, N.H. Kim, J. Appl. Phys. 73 (1993) 5677–5679.
[26] A.I. Akhiezer, V.G. Baryakhtar, M.I. Kaganov, Uspechi Fiz. Nauk 71 (1960) 533.
[27] Ł. Gondek, A. Szytuła, M. Bałanda, W. Warkocki, A. Szewczyk, M. Gutowska, Solid State Commun. 136 (2005) 26–31.
[28] S. Baran, D. Kaczorowski, A. Arulraj, B. Penc, A. Szytuła, J. Magn. Magn. Mater. 321 (2009) 3256–3261.
[29] W. Sikora, F. Białas, L. Pytlik, J. Appl. Crystallogr. 37 (2004) 1015–1019.